Article

Feasibility study of a new Cherenkov detector for improving volcano muography

Domenico Lo Presti [1,2†,‡], Giuseppe Gallo [1,3,‡,*], Danilo L. Bonanno [2,†,‡], Daniele G. Bongiovanni[‡], Fabio Longhitano and Santo Reito [2,‡]

[1] Department of Physics and Astronomy "E. Maiorana", University of Catania, Via S. Sofia 64, 95123 Catania Italy
[2] INFN, Sezione di Catania, Via S. Sofia 64, 95123 Catania Italy
[3] INFN, Laboratori Nazionali del Sud, Via S. Sofia 62, 95123 Catania Italy
* Correspondence: gallog@lns.infn.it
† Current address: Via S. Sofia 64, 95123 Catania Italy
‡ These authors contributed equally to this work.

Version January 21, 2019 submitted to Preprints

Abstract: Muography is an expanding technique for the investigation of the internal structure of targets of interest in geophysics. The flux of high penetrating muons produced by primary cosmic rays is attenuated by traversing kilometer size objects like X-ray flux is attenuated through the human body. This gives the possibility to study the internal structure of volcanoes or underground cavities, e.g., starting from the measure of the muon flux transmission through the target. Many groups of researchers working with this technique have to face with high background level that afflicts the reconstruction of muon tracks near the horizontal direction. An important source of background is the scattering of particles near the detector that produces a wrong reconstruction of the incoming direction. An innovative technique based on Cherenkov radiation was investigated by means of Monte Carlo simulations developed in Geant4 toolkit and MATLAB. The results reported in this paper show that the presented technique is able to correctly distinguish the incoming direction of particles with an efficiency higher than 98%. This new kind of detector could represent an alternative for high resolution charged particle tracking also for other applications.

Keywords: Muography; Cherenkov radiation; Monte Carlo; Geant4; MATLAB; Particle detectors

1. Introduction

Muon radiography - or briefly muography - is a promising technique which aims at resolving the internal structure of large size objects by taking advantages of the high penetrating power of cosmic muons. Although the properties of muons interaction with matter have been known for a long time, the investigation of their potential as a probe to give information of large structures is a recent development. In the last years it is possible to found an increasing number of paper discussing the application of muography to target as volcanoes, underground cavities and also pyramids with impressive results [1–6].

The muography technique is based on the reconstruction of the incident direction of the detected muons after crossing the target object. The basic element for a muography experiment is a tracker detector with at least two position sensitive planes in order to reconstruct the particle tracks. The incoming direction of the muons entering the detector may be distinguished from the slope of the reconstructed trajectory, assuming that the muon flux is downward oriented only. In this circumstance, muons detected, after being scattered near the detector and crossing it upward oriented, will be wrongly reconstructed. This contamination, together with the other sources of background, produces an overestimation of the muon counts that could be critical when compared with an very tiny expected flux.

A proposed solution to overcome this source of background is the time-of-flight (TOF) measurement of the muons in traversing the detector [7,8]. The muon incoming direction can be

distinguished by the difference between the detection time Δt in the external tracking planes of the detector. Being the path, between the two detection points, dependent on the angle between the particle trajectory and the normal to the telescope planes, the time distribution will be characterized by two lobes for $\Delta t > 0$ and $\Delta t < 0$, respectively, with a superimposition for $\Delta t \simeq 0$, corresponding to particles perpendicular to the detection planes, which depends on time measurement resolution. Hence, for muons traveling the minimum distance in traversing the detector an uncertainty remains about their incoming direction.

In this paper an alternative solution for this problem, based on the directionality of Cherenkov emission, is investigated by means of Monte Carlo simulations. The detector was designed as a possible upgrade of the muon telescope already working, developed inside the MEV project [9]. It consist of two adjacent radiator plates in which Cherenkov emission produced by muons takes place. The plates are separated by a foil of light absorbing material in order to prevent the Cherenkov radiation generated in a radiator from escaping and entering into the other one or could be reflected back. The two opposite faces of the detector are instrumented with light sensors to reveal the Cherenkov emission. The working principle is quite simple: the Cherenkov radiation should be revealed only in the second radiator traversed by the particle, in which the light is emitted toward the instrumented face of the plate.

Different configurations of the Cherenkov detector were simulated by means of the Geant4 toolkit, changing the plate thickness and the number and arrangement of the light sensors. The results, reported in the following, show that the incoming direction of the muons can be distinguished with an efficiency of 98% for the best simulation scenario. Meanwhile, the possibility to develop a stand-alone muon telescope based on Cherenkov emission was considered and the tracking performance of this detector were studied, showing promising results also for other charged particle tracking applications.

2. Results

The design of the new detector under study is shown in figure 1. This is a module composed of two radiator of transparent material with size $20 \times 240 \times 240$ mm^3. In sight of a possible upgrade for the MEV project telescope, with a sensitive area of 1 m^2, the final Cherenkov tag detector will be composed of a square matrix of 16 single modules to cover the sensitive area. The opposite side of each plate is equipped with light sensors to detect the Cherenkov radiation emitted in the corresponding radiator, while the lateral faces are coated with the same light absorbing material that separates the two plates.

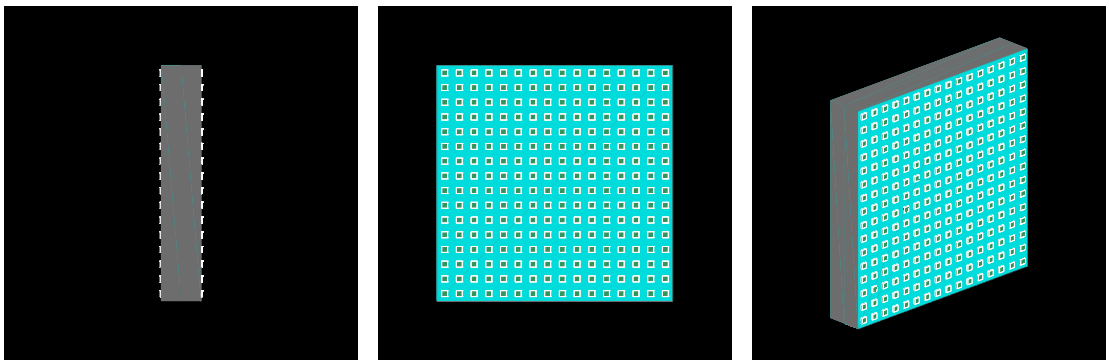

Figure 1. Lateral, front and perspective visualizations of the detector simulated in Geant4 for the configuration with a 16×16 array of SiPMs (6×6 mm^2 sized) for the optical readout of each sensitive face. The size of each radiator are $20 \times 240 \times 240$ mm^3.

The Cherenkov threshold is usually given in terms of the ratio between particle velocity and the speed of light, $\beta_{th} = 1/n$, where n is the refractive index of the medium. Since $E = \gamma m_0 c^2$ and $\gamma = \left(1 - \beta^2\right)$, the threshold can be expressed as:

Preprints (www.preprints.org) | NOT PEER-REVIEWED | Posted: 21 January 2019 doi:10.20944/preprints201901.0203.v1

Peer-reviewed version available at Sensors 2019, 19, 1183; doi:10.3390/s19051183

$$E_{th} = \frac{m_0 c^2}{\sqrt{1 - \frac{1}{n^2}}}, \tag{1}$$

in which is evident the dependence on particle rest mass m_0. The mechanism of Cherenkov effect confines the photons to a cone with its vertex coincident with the point of first light emission. Also the aperture angle θ_C of the light cone is related to the particle velocity and to the refractive index of the medium according to the equation

$$\cos\theta_C = \frac{1}{n\beta}. \tag{2}$$

With this in mind, it is possible to imagine what happens when a particle enters the detector from an instrumented side. The emission of Cherenkov photons immediately begins if the particle energy is over the typical threshold and the photons produced in the first radiator will be directed toward the light absorbing foil and will stop in it. Then, the particle enters the second radiator and the photons, in this case, will be emitted in the direction of the light sensitive surface. An example of the described interaction between a muon with kinetic energy equal to 10^5 MeV at the starting point, located at the left side of the detector, is shown in figure 2.

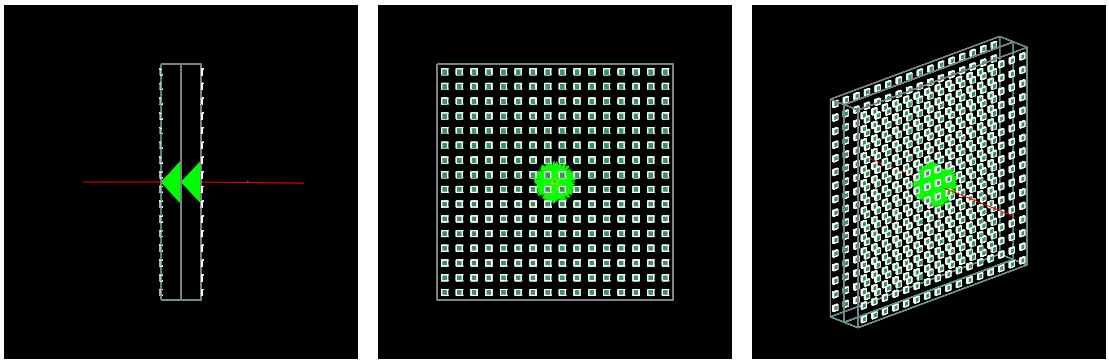

Figure 2. Lateral, front and perspective visualizations of event of a muon with kinetic energy 10^5MeV simulated in Geant4 for the configuration shown in fig.1. The optical photons internally reflected at the interface between Plexiglas and air were suppressed to simplify the scene. Respect to fig. 1, plexiglass and light absorbing foils are drawn only as wire-frame in order to visualize photons trajectories inside.

2.1. Feasibility study for incoming particle direction discrimination

The feasibility of the just exposed idea was verified by means of an extensive series of Monte Carlo simulations. The material chosen for the radiator was Plexiglas, with a refraction index slightly varying from 1.481 to 1.505 with increasing photons energies from 1.145 eV to 3.064 eV. For a value of the refraction index equal to 1.49 at the wavelength of nearly 600 nm, the energy thresholds for Cherenkov emission are $E_{th}(\mu) = 142.525$ MeV, $E_{th}(e^-/e^+) = 0.689$ MeV, $E_{th}(p) = 1265.66$ MeV, for muons, electrons/positrons and protons respectively.

The light sensitive side of each radiator is instrumented with SiPMs of 6×6 mm^2. The best strategy to distinguish the incoming direction of the particle was established by studying the number of SiPMs that produce a signal higher than a suitable threshold on each side of the detector, which in the following will be indicated as SiPM "fired".

The results of each set of simulation is reported as the percentage of successful recognized directions ("Successful tagged"). An event is considered well reconstructed when the discrimination condition is satisfied by only one instrumented side of the detector. The failure rate stands for the percentage of events when both instrumented sides pass the discrimination test - and it is impossible to establish which of them is the correct side - or no one. This last scenario is useful to take into account

border effects, i.e. particles that enter the detector from an instrumented face and exit the second radiator from a lateral side covered by coating foil; the Cherenkov light cone is directed, partially or completely, toward the lateral side and there are not sufficient photons to trigger the discrimination condition. In this case the incoming direction is not recognized at all. Furthermore, it is possible that no side passes the discrimination condition for low energy muons, when the angular aperture of the Cherenkov light cone is too low to hit a sufficient number of SiPMs or when β of the particles is under threshold. The mean number of SiPMs fired for each event is also included in the results.

Four different detectors set-up were simulated, varying the size of the radiators and/or the number of SiPMs. In every case, the light sensors were placed following a regular pattern with SiPMs equally spaced. The simulated arrangements are:

- Radiator size $30 \times 240 \times 240$ mm^3, 13×13 SiPMs array;
- Radiator size $20 \times 240 \times 240$ mm^3, 13×13 SiPMs array;
- Radiator size $20 \times 240 \times 240$ mm^3, 16×16 SiPMs array;
- Radiator size $20 \times 240 \times 240$ mm^3, 20×20 SiPMs array.

Excluding the second set-up in which the number of SiPMs was insufficient, in every case the failure rate is lower than 2% for muons with energy above $E_{th}(\mu)$. The results for successful configurations are reported in figure 3. These results were obtained with two primary particle sources, one for each entrance face of the detector, with the same geometric configuration. Each run of the simulation consists of 1000 muons shot randomly from one the two sources and with random direction, with angular distribution limited in order to hit the detector.

The analysis of the simulations output was developed in MATLAB software environment, by means of which the figures that summarize the results were produced. It is possible to notice that for each subplot of figure 3 there are two different data series, one for Cherenkov photons and the other for photo-electrons (p.e.) generated after applying the "digitization" procedure that takes into account the SiPMs properties, including dark noise, described in detail in the following.

For each scenario the best parameters for direction tagging were found and the results of figure 3 refer to the following conditions: the threshold to consider a SiPM "fired" is equal to 5 photons or p.e., respectively; the number of sensors fired on a single side has to be higher than 1, or 2 only for the case of 20×20 SiPMs, to assign uniquely the incoming direction.

2.2. High resolution position measurement

The possibility to use the same detector for other purposes beyond the incoming direction tagging was also studied. In particular, the possibility to reconstruct the position of the crossing muon from the SIPMs signal was investigated. The very promising results of this study are reported in figure 4. The muon position at the exit point from the radiator was reconstructed by means of a two-dimensional Gauss fit on the matrix of the number of p.e. counted by each SiPM. The mean distance between the muon exit point and the centroid obtained from fit is between 2.0 and 4.5 mm, depending on the SiPM arrangement. This result could represent a strong enhancement for muography applications by means of an high resolution reconstruction of the tracks.

Starting from the showed results, it is possible to affirm that the extensive simulations study conducted by means of Geant4 and MATLAB proves the principle of the proposed new technique for background discrimination in muography experiment. The efficiency of the set-up depends on the thickness of the radiator and on the number and arrangement of the SiPMs, but various configurations were found which give a failure rate lower than 2% at saturation energy. In fact, in each case for muons kinetic energies higher than 120 MeV, the mean number of SiPMs fired becomes constant, considering statistical fluctuations, and the efficiency follows a similar trend.

3. Discussion

The detector was initially ideated as an upgrade for the muon tracker telescope already built and operating inside the MEV project [9]. The Cherenkov direction discrimination prototype implemented

Preprints (www.preprints.org) | NOT PEER-REVIEWED | Posted: 21 January 2019 doi:10.20944/preprints201901.0203.v1

Peer-reviewed version available at Sensors 2019, 19, 1183; doi:10.3390/s19051183

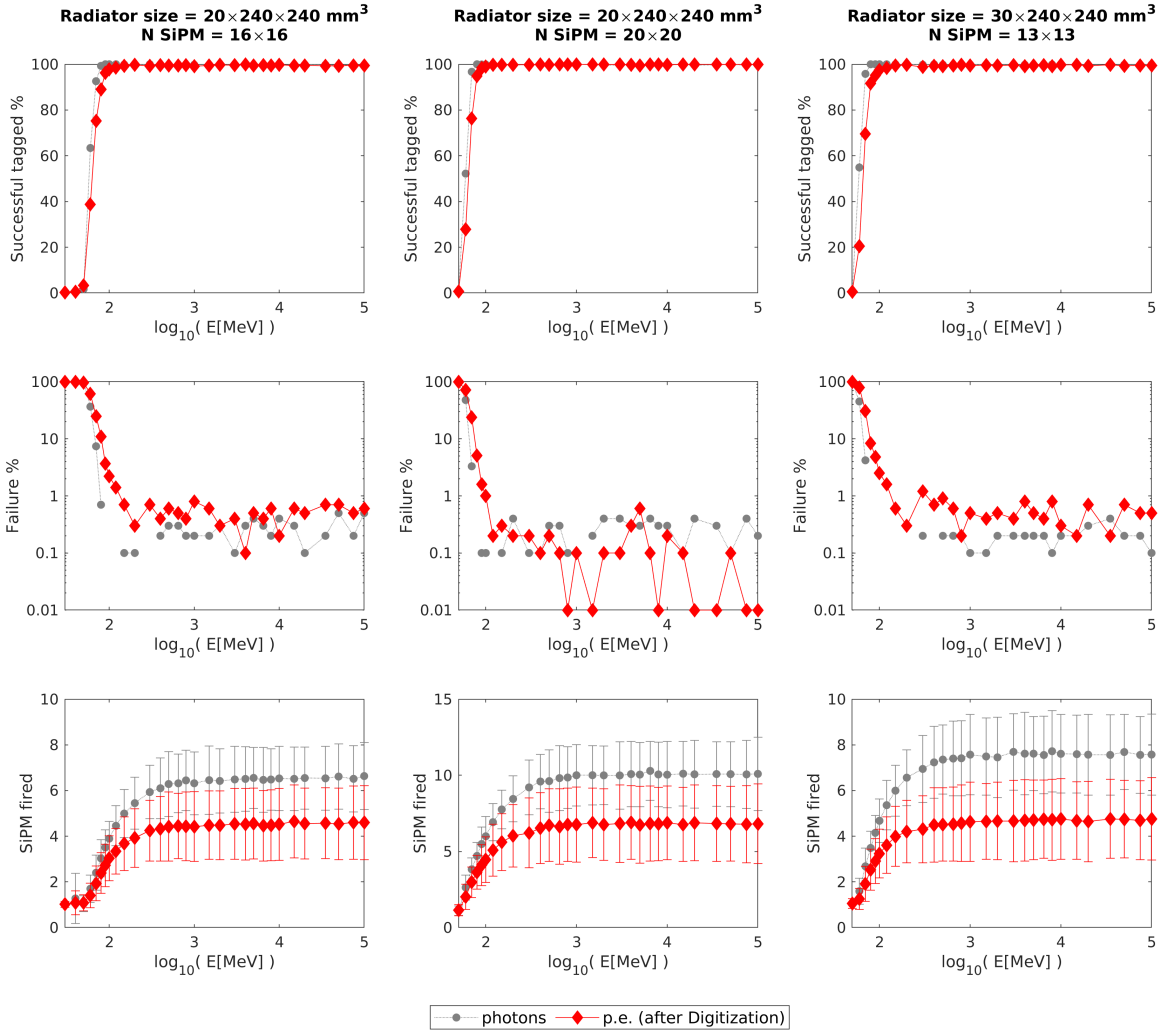

Figure 3. Results of Geant4 simulation as a function of the kinetic energy E of the primary particles (muons). Each column of subplot refers to a different simulation scenario, in which radiator size and/or number of SiPM have changed, as shown in the title.

in the simulation was a reduced scale version of the final detector. Plexiglas was chosen as radiator material to ensure high transparency to Cherenkov light, even if the UV wavelengths are cut down because its absorption length drops from several meters to only few millimeters in this spectral region.

From the careful study of the simulation was observed that Cherenkov light emission by muons was not the unique relevant physical process. In fact, with a probability that depends on primary particle energy, muons can interact with the radiator medium, generating electrons by scattering. The energy of the scattered electrons, which depends, in turn, on the energy of primary particle, is of the order of 10^3 keV for the simulated muon energies. Since the energy of secondary electrons is higher than threshold for these particles, as established by equation (1), they generate Cherenkov radiation too. The electrons are emitted randomly because of the nature of the scattering process, their number is limited to some tens and their path through the medium is short. Taking into account all that, the signal produced by secondary electrons is very low respect to that of Cherenkov photons induced by fast muons and can be confused with the noise introduced by the digitization process in the SiPMs.

Instead, for primary particle with energy lower than threshold, Cherenkov photons could be produced by scattered electrons only and they could mimic the signal of a higher energy muon leading to a wrong reconstruction of the incoming direction. This scenario was studied for the set-up with radiator of $20 \times 240 \times 240$ mm^3 and an array of 16×16 SiPMs starting from 30 MeV for the energy

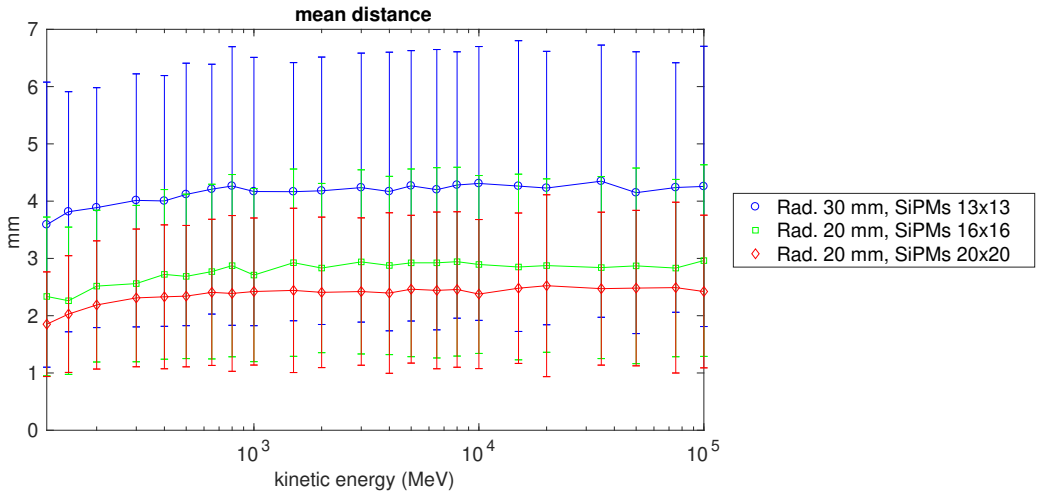

Figure 4. Mean distance between muon exit point from the radiator and 2D Gauss fir centroid in mm, for energies from 120 MeV to 10^5 MeV. In the legend are reported the radiator width in mm and the number of SiPMs in the array of sensors on the opposite face of the two radiator. The vertical error bars represent the standard deviation of each mean distance distribution.

spectrum. Slow muons loss all or the major part of their kinetic energy into the radiator and experience a strong Multiple Coulomb Scattering (MCS) such that they are heavily deflected respect their incoming directions or completely stopped in the detector. If we consider a system with two tracking planes and a direction discrimination detector in the middle of them, slow muons will not be a problem because after traversing the Cherenkov radiator they will be scattered outside the field of view of the whole system and, without coincidence on the second tracking plane, the acquisition of the signal will not be triggered. Otherwise, if a slow muon deflects and hit anyway both tracking planes, a linear fit discrimination will reject this event because the three impact points will be not aligned. Indeed, shutting down the signal produced by muons deflected more than 1°, the efficiency is nearly zero, i.e. the discrimination of the incoming direction works as expected. The few failures are due to the digitization noise.

Regarding the position measurement, the resolution of a single tracking module is higher than that of every system based on scintillating strips because the measure of the position is continuous and not discrete due to strips size. Until now, the continuous measure of the position in muography experiment was performed only by means of detector based on multi-wire proportional chamber (MWPC) or with nuclear emulsions, but with the latter the time information is inaccessible. In order to compare the performance of a muon tracker completely based on the new technique proposed in this paper with an apparatus like that described in ref. [5], it is required, at least, a simulation that includes three or more tracking planes, but this is beyond the scope of this work.

If only the results about the capability of direction discrimination are considered, it will be difficult to establish which of the simulated configurations is the best. The main difference between them is the energy where the efficiency reaches a stable value greater than 98%. In a muography experiment to investigate the internal structure of large object such a volcano, the particles with low energy can be misleading because they are strongly deflected by MCS and their trajectory could be wrongly back-projected. This consideration, together with the advantage of limited number of electronic channels for signal read-out, could lead to chose the set-up with a thicker radiator and a lower number of SiPMs.

But if the purpose of the system includes the position measurement, a closer spacing between light sensors will be useful. The configuration with two radiators, each 20 mm thick, and a regular array with 16×16 SiPMs is the best between the ones investigated because it reaches approximately

the same efficiency of the set-up with a higher number of sensors and the resolution on the position measurement is slightly worst despite nearly only two third of SiPMs are used.

Next step will be the comparison between experimental results in a reduced scale prototype and simulations. A $20 \times 60 \times 60$ mm^3 size prototype is under construction. Many solutions for the material of the radiator and the front-end electronics will be tested. For example, the use of optical gel in place of the plexiglass, could improve the transmission for UV Cherenkov photons and the optical coupling to PS optical window. The need for the measure of the number of photons detected by each SiPM, instead of a simple threshold, imposes severe constraints in the electronic chain regarding dead time and trigger strategy.

4. Methods

The simulations were performed using Geant4 [10], a toolkit for simulation of the passage of particles through matter. This toolkit is not specifically developed to work as a ray-tracer, but was chosen for this task because it accomplishes the generation of optical photons according the physical process involved in the interaction between a medium and a primary particle from the source.

Geant4 provides a general model framework that allows the implementation of alternative physical models to describe the same process. In order to keep the simulation more general as possible and avoid to neglect some unexpected physical processes, the Physics List uses the approach of `G4VModularPhysicsList`. Technically speaking, a physics list can be implemented by specifying all the necessary particles and attaching to them the associated physics processes, but this requires a complete understanding of the whole physics involved. `G4VModularPhysicsList`, that is a sub-class of `G4VUserPhysicsList`, allows a user to organize physics processes into "building block", or "modules", and compose a physics list of such modules. This concept allows to group together desired combination of selected particles and related processes. The modules included into the physics list of the simulations discussed here are:

- `G4EmStandardPhysics`;
- `G4DecayPhysics`;
- `G4EmExtraPhysics`;
- `G4HadronElasticPhysics`;
- `G4HadronPhysicsFTFP_BERT`;
- `G4OpticalPhysics`.

A description of the available physics models and processes within the Geant4 toolkit can be found in ref. [11].

4.1. Detector construction

Both radiator tiles are made of Plexiglas ($C_5H_8O_2$, density $= 1.19\,\mathrm{g/cm^3}$) with sizes 240×240 mm^2 along y and z coordinates and 20 or 30 mm along x coordinate. Each tile has the lateral faces, those perpendicular to y and z axes, coated with a thin foil of polyvinyl chloride (PVC, $C_2H_2Cl_2$, density $= 1.7\,\mathrm{g/cm^3}$), 180 µm thick. One of two wider faces, perpendicular to x axis, is also coated with PVC foil, whereas the other one is left uncovered in order to allow the optical coupling with the light sensors. The two plates are arranged such that the larger coated surfaces face each other in contact.

Each SiPM is constructed as a mother volume whit sizes $1.45 \times 6.0 \times 6.0$ mm^3, along x, y and z coordinates respectively, made of Silicon (Si). A second thinner box is placed inside the mother volume, with sizes $0.3 \times 6.0 \times 6.0$ mm^3, aligned along the x coordinate to a surface of the Si box. This inner volume represents the photosensitive window of the SiPM and is made with epoxy resin (CHO, density $= 1.0\,\mathrm{g/cm^3}$). The "photosensitive surface" (PS) is a metal slab at the back end of the epoxy box that is only a very rough approximation of the real thing since it only absorbs or detects the photons based on its efficiency. The SIPMs are placed with the epoxy window faced to the uncoated surface of the radiator and arranged as an equally spaced $N_S \times N_S$ square array.

The world volume, which contains all the other volumes, is filled with air.

4.2. Optical properties

In order to correctly simulate the transportation of optical photons, Geant4 requires the user to provide the optical properties for both bulk materials and surfaces between them. This is a crucial point about processes involving optical photons, because without a documentation or a measure of the optical properties of the materials the optical physics processes will not be activated. The main parameters used in the simulations are listed in table 1.

Optical properties	
Refractive index of Air	1.00
Refractive index of Plexiglass	$1.481 - 1.505$
Absorption length of Plexiglass	$5.40\,\text{m} - 1\,\text{mm}$
Refractive index of Epoxy	1.55
Absorption length of Epoxy	$4.20\,\text{m} - 1\,\text{mm}$
Efficiency of PS	1.00
Reflectivity of PS	0.05

Table 1. Materials and surfaces optical properties implemented in the simulations. When two values are specified, the corresponding optical property varies with photon energies that spans from 2.00 to 4.136 eV.

When a photon arrives at a medium boundary its behavior depends on the nature of the materials that compose it. Surface boundaries may be formed between two dielectric materials or between a dielectric and a metal. They can be defined in two ways: between two specific volume (`G4LogicalBorderSurface`) or around one volume (`G4LogicalSkinSurface`). The first requires that the two volume forming the surface and their optical properties have to be specified by the user. If a `G4LogicalSkinSurface` is attached to a volume, its properties are applied to every surface of it.

When a `G4OpticalSurface` is defined, the user can specify `G4OpticalSurfaceModel`, i.e. the reflection physics model, `G4OpticalSurfaceFinish` and `G4OpticalSurfaceType` between dielectric-dielectric and dielectric-metal. The Geant4 code allows the user to select one of the two optical reflection models, the `glisur` model and the `unified` one. The `glisur` model assumes that the surface is made of micro-facets, where a micro-facet is randomly selected from a distribution each time a reflection occurs. The specular reflection is calculated based on the micro-facet orientation. In the unified model four kinds of surface reflection are possible: specular spike, specular lobe, backscatter and lambertian. If no `G4OpticalSurface` is defined, the reflection is simulated as a geometric reflection at a perfectly smooth optical surface, i.e. applying Snell's law. The surface finish can be set among:

- `polished`, smooth perfectly polished surface;
- `polishedfrontpainted`, polished top-layer paint;
- `polishedbackpainted`, polished (back) paint/foil;
- `ground`, rough surface;
- `groundfrontpainted`, rough top-layer painted;
- `groundbackpainted`, rough (back) paint/foil.

In the simulations, the properties for the two defined surface boundaries were kept constant. A `G4LogicalBorderSurface` was specified between each radiator and the PVC wrapping, with optical surface properties specified as:

- `G4OpticalSurfaceModel`: `unified`;
- `G4OpticalSurfaceFinish`: `polishedbackpainted`;
- `G4OpticalSurfaceType`: `dielectric_dielectric`.

A `G4LogicalSkinSurface` around the epoxy window volume with the following optical surface properties:

- `G4OpticalSurfaceModel`: `glisur`;
- `G4OpticalSurfaceFinish`: `polished`;
- `G4OpticalSurfaceType`: `dielectric_metal`.

A more detailed explanation about simulation of optical physics in Geant4 can be found in ref. [12].

4.3. Digitization

The analysis of the simulation output was developed in MATLAB. The number of generated photons which reach the PS at the back-layer of the epoxy window is counted. This number takes into account both Cherenkov radiation produced by primary muons and the one due to secondary electrons. The digitization procedure is needed to convert the number of photons, N_{ph}, in the given event, into the number of p.e. generated in SiPM. Because the structure of the SiPM is not simulated, a statistical approach is required for the conversion. The number of p.e., N_{pe}, is random generated from the Poisson distribution with mean parameter N_{ph} and takes into account the photon detection efficiency (PDE) and the fill factor f of the SiPM, as $N_{pe} = \texttt{poissrnd}(N_{ph}) \times \text{PDE} \times f$, where $\texttt{poissrnd}\,(\lambda)$ is the MATLAB function to extract random number from Poisson distribution with mean parameter λ. PDE and f are set equal to 0.5 and 0.74 respectively. The digitization procedure adds also a Gaussian noise to the signal, with mean and sigma equal to 2 and 1 respectively, in order to mimic the dark current rate of the SiPM.

4.4. Position measurement

When the incoming direction of the primary muons is correctly discriminated, an additional analysis can be done on the matrix of N_{pe} for each SiPM of the instrumented radiator side which passes the discrimination test. It consists of a surface fit on 3D set of points. The y and z coordinates of the SiPM center positions are set as independent variables, while the corresponding $N_{pe}(y,z)$ was the dependent one. The two-dimensional fit function is a 2D rotated Gaussian:

$$N_{pe}(y,z) = a + b\ \exp\left\{-\left[\frac{(y-c_1)\ \cos(t1)+(z-c_2)\sin(t_1)}{w_1}\right]^2 - \left[\frac{-(y-c_1)\sin(t_1)+(z-c_2)\cos(t_1)}{w_2}\right]^2\right\}, \quad (3)$$

with the following parameters:

- a, offset along N_{pe} coordinate;
- b, amplitude of the 2D gaussian;
- c_1, centroid y coordinate of the 2D gaussian;
- c_2, centroid z coordinate of the 2D gaussian;
- t_1, angle of rotation for the 2D gaussian;
- w_1, width along y of the 2D gaussian;
- w_2, width along z of the 2D gaussian.

The reconstructed position of a muon going out the last radiator along its path is assigned equal to (c_1, c_2) on the (y,z) plane at x equal to the border of the radiator. Then the distance between (c_1, c_2) and the true exit position of the muon, retrieved from the simulation output is calculated to investigate the precision of this measurement, as showed in fig. 4.

5. Conclusions

In conclusion, it is possible to affirm the the feasibility study conducted and exposed in this paper opens a new promising possibility to reduce the background noise in muography applications. The working principle of the Cherenkov tag detector works well in simulations. Even if other aspetcs could be investigated, the next fundamental steps will be a comparison and a fine tuning between

simulations and the experimental study of a prototype, which include many technical constrains not reproducible in simulations.

Author Contributions: Conceptualization D.L.P.; software G.G.; writing-review and editing D.L.P. G.G. and D.L.B.; all the authors contributed to investigation, validation and data processing.

Funding: This research received no external funding.

Conflicts of Interest: The authors declare no conflict of interest.

1. Tanaka, H.K.M.; Nakano, T.; Takahashi, S.; Yoshida, J.; Takeo, M.; Oikawa, J.; Ohminato, T.; Aoki, Y.; Koyama, E.; Tsuji, H.; Niwa, K. High resolution imaging in the inhomogeneous crust with cosmic-ray muon radiography: The density structure below the volcanic crater floor of Mt. Asama, Japan. *Earth and Planetary Science Letters* **2007**, *263*, 104–113. doi:10.1016/j.epsl.2007.09.001.
2. Lesparre, N.; Gibert, D.; Marteau, J.; Komorowski, J.C.; Nicollin, F.; Coutant, O. Density muon radiography of La Soufrière of Guadeloupe volcano: comparison with geological, electrical resistivity and gravity data. *Geophysical Journal International* **2012**, *190*, 1008–1019. doi:10.1111/j.1365-246X.2012.05546.x.
3. Morishima, K.; Kuno, M.; Nishio, A.; Kitagawa, N.; Manabe, Y.; Moto, M.; Takasaki, F.; Fujii, H.; Satoh, K.; Kodama, H.; et al. Discovery of a big void in Khufu's Pyramid by observation of cosmic-ray muons. *Nature* **2017**, *552*, 386–390. doi:10.1038/nature24647.
4. Saracino, G.; Amato, L.; Ambrosino, F.; Antonucci, G.; Bonechi, L.; Cimmino, L.; Consiglio, L.; D'Alessandro, R.; Luzio, E.D.; Minin, G.; et al. Imaging of underground cavities with cosmic-ray muons from observations at Mt. Echia (Naples). *Scientific Reports* **2017**, *7*, 1181. doi:10.1038/s41598-017-01277-3.
5. Oláh, L.; Tanaka, H.K.M.; Ohminato, T.; Varga, D. High-definition and low-noise muography of the Sakurajima volcano with gaseous tracking detectors. *Scientific Reports* **2018**, *8*, 3207. doi:10.1038/s41598-018-21423-9.
6. Tanaka Hiroyuki K. M..; Oláh László. Overview of muographers. *Philosophical Transactions of the Royal Society A: Mathematical, Physical and Engineering Sciences* **2019**, *377*, 20180143. doi:10.1098/rsta.2018.0143.
7. Jourde, K.; Gibert, D.; Marteau, J.; de Bremond d'Ars, J.; Gardien, S.; Girerd, C.; Ianigro, J.C.; Carbone, D. Experimental detection of upward going cosmic particles and consequences for correction of density radiography of volcanoes. *Geophysical Research Letters* **2013**, *40*, 6334–6339. doi:10.1002/2013GL058357.
8. Cimmino, L.; Ambrosino, F.; Bonechi, L.; Ciaranfi, R.; D'Alessandro, R.; Masone, V.; Mori, N.; Noli, P.; Saracino, G.; Strolin, P. The MURAVES telescope front-end electronics and data acquisition. *Annals of Geophysics* **2017**, *60*, 0104. doi:10.4401/ag-7379.
9. Lo Presti, D.; Gallo, G.; Bonanno, D.L.; Bonanno, G.; Bongiovanni, D.G.; Carbone, D.; Ferlito, C.; Immè, J.; La Rocca, P.; Longhitano, F.; et al. The MEV project: Design and testing of a new high-resolution telescope for muography of Etna Volcano. *Nuclear Instruments and Methods in Physics Research Section A: Accelerators, Spectrometers, Detectors and Associated Equipment* **2018**, *904*, 195–201. doi:10.1016/j.nima.2018.07.048.
10. Agostinelli, S.; Allison, J.; Amako, K.; Apostolakis, J.; Araujo, H.; Arce, P.; Asai, M.; Axen, D.; Banerjee, S.; Barrand, G.; et al. Geant4—a simulation toolkit. *Nuclear Instruments and Methods in Physics Research Section A: Accelerators, Spectrometers, Detectors and Associated Equipment* **2003**, *506*, 250–303. doi:10.1016/S0168-9002(03)01368-8.
11. User Support | geant4.web.cern.ch.
12. Dietz-Laursonn, E. Peculiarities in the Simulation of Optical Physics with Geant4. *arXiv:1612.05162 [physics]* **2016**. arXiv: 1612.05162.